Zerihun et al., Irrigat Drainage Sys Eng 2018, 7:3
DOI: 10.4172/2168-9768.1000222

Irrigation & Drainage Systems Engineering

Research Article Open Access

Slope Effects on the Pressure Head Profile Patterns of Sprinkler Irrigation Laterals, II. Evaluation Based on Simulation

Zerihun D[1]*, Sanchez CA[2] and Bautista E[3]

[1]Maricopa Agricultural Center, University of Arizona, 37860 W. Smith-Enke Rd, Maricopa, AZ, USA
[2]Department of Soil, Water and Environmental Science and Maricopa Agricultural Center, University of Arizona, USA
[3]Research Hydraulic Engineer, USDA-ARS Arid-Lands Agricultural Research Center, Maricopa, USA

Abstract

Theoretical analysis of slope effects on the spatial patterns of the pressure head profiles of an irrigation lateral is presented in the companion paper. Results of the analysis are evaluated here based on simulations. Simulations were conducted for data sets covering a wide range of lateral parameters. The results show that the pressure profile patterns of a lateral, and possibly the locations of the pressure extrema along the lateral, can be determined by comparing the negative lateral slope with the friction slope at the inlet and/or distal ends, confirming an important inference of the analysis. The simulation study also shows that the full range of variation of lateral pressure profile patterns can be differentiated into the three distinct categories defined based on theory. While results of the analysis developed in the companion paper are generally true, they nonetheless produce only particular solutions (i.e., solutions specific to a given lateral slope). The simulation results, however, provide additional insights, into the relationships between slopes and pressure profile patterns, which would enhance the practical significance of the theoretical analysis. For each data set, considered, simulation outputs reveal that there exists a unique pair of threshold slopes that delimits the feasible range of variation of the lateral slope into three subintervals, each with a specific lateral pressure head profile pattern. Furthermore, the spatial pattern of the simulated lateral pressure profiles, within each of these slope subintervals, corresponds to one of the three categories defined in the companion paper. Hence, the full range of variation of the lateral pressure profile patterns can be completely characterized based on a pair of threshold slopes that are unique to the lateral, which is an advantage. Results of the simulation study are, nonetheless, empirical. Thus, more comprehensive studies are needed to conclusively establish the broader significance of these results.

Keywords: Friction slope; Lateral slope; Step function; Pressure slope; Stationary point

Notations

The following notations are used in this paper:

$h(x,\psi_i)$ = Pressure head profile (i.e., function that relates pressure head with distance from lateral inlet) for a lateral slope of ψ_i;

$h'(x,\psi_i)$ = Pressure slope profile (i.e., function that relates the slope of the pressure head profile with distance from lateral inlet) for a lateral slope of ψ_i;

$H_f'(x,\psi_i)$= Friction slope profile (i.e., function that relates the slope of the friction head loss profile with distance from lateral inlet) for a lateral slope of ψ_i;

h = Pressure head profile;

h' = Pressure slope profile;

H_f' = Friction slope profile;

x = Distance from lateral inlet;

ψ = Lateral slope.

Introduction

Mathematical modeling and analysis of the hydraulics of irrigation laterals have been the subject of various studies [1-6]. Application of models in the hydraulic design of sprinkler and drip irrigation laterals has been explored by various authors [7-12]. However, the study reported here is focused on the analysis of the spatial patterns of the pressure head profiles of sprinkler irrigation laterals as affected by slope. Theoretical analysis of slope effects on lateral pressure head profile patterns are described in the companion manuscript [13] and verification of the theoretical results are presented here.

The effect of slope on pressure head variability along an irrigation lateral is typically limited. However, for a lateral with given hydraulic and geometric characteristics there exists a well-defined relationship between lateral slope and the spatial pattern of the corresponding pressure head profile [13]. Thus, a sound understanding of these relationships can be useful in the verification of lateral hydraulic models and design recommendations.

Slope effects on lateral pressure head extrema and their locations along a lateral have been studied in the context of the hydraulic design of laterals. Wu et al. [14] used a set of criteria, developed based on the ratio of elevation differential to friction head loss along a lateral, to differentiate the pressure head profile patterns of a drip irrigation lateral into distinct categories. Keller and Bleisner [8] described slope effects on lateral pressure head extrema and the average lateral pressure head in the context of lateral design. Scaloppi and Allen [3], and Yildirim [15] proposed equations for calculating maximum and minimum pressure heads and their locations along a lateral assuming continuous and uniform and/or continuous and non-uniform spatial distributions of outflow discharge along the lateral. Martin et al. [16] presented a set of criteria for determining pressure head extrema and their locations along a lateral.

***Corresponding author:** Zerihun D, Associate Research Scientist, Maricopa Agricultural Center, Univ. of Arizona, 37860 W. Smith-Enke Rd., Maricopa, AZ 85138-3010, USA, Tel: +520-374-6221; E-mail: dawit@ag.arizona.edu

Received August 30, 2018; **Accepted** December 13, 2018; **Published** December 20, 2018

Citation: Zerihun D, Sanchez CA, Bautista E (2018) Slope Effects on the Pressure Head Profile Patterns of Sprinkler Irrigation Laterals, II. Evaluation Based on Simulation. Irrigat Drainage Sys Eng 7: 222. doi: 10.4172/2168-9768.1000222

The theoretical analysis of slope effects on lateral pressure head profiles patterns, presented in the companion paper, assumes that the lateral parameter set constitutes a feasible hydraulic scenario and is spatially invariant. Results of the analysis are evaluated here based on hydraulic simulations. Accordingly, a simulation study was conducted based on three different data sets covering a wide range of lateral hydraulic and geometric characteristics. For each data set, multiple simulations were performed with a numerical model, developed by Zerihun and Sanchez (6), by varying the lateral slope over a sufficiently wide interval such that the resultant pressure head profile patterns cover the full range of variation defined in the companion manuscript.

For each data set, the results show that the pressure head profile pattern of a lateral, and possibly the locations of the pressure head extrema along the lateral, can be determined based on a comparison of the negative of the lateral slope with the corresponding friction slopes at the inlet and/or distal ends of the lateral. Note that this confirms an important inference of the theoretical analysis presented in the companion paper. Outputs of the simulation also show that the full range of variation of the pressure head profile patterns of a lateral is comprised of the three distinct categories defined in the companion paper based on theoretical analysis.

Furthermore, results of the hydraulic simulations provide additional insights, of some practical significance, into the relationships between lateral slopes and pressure head profile patterns. The simulation results reveal that, for each data set, there exists a unique pair of threshold slopes (referred here as the lower and upper threshold slopes) that delimits the slope range into three subintervals, each with a particular pressure head profile pattern. The results also show that the spatial patterns of the pressure head profiles, within each of these slope subintervals, corresponds to one of the three categories defined in the companion paper. The implication is that the full range of variation of the pressure head profile patterns of a lateral can be characterized based on a pair of threshold slopes that are unique to the lateral.

The results of the theoretical analysis presented in the companion paper are generally true. However, they produce only particular solutions, i.e., solutions specific to a given lateral slope. In other words, with this approach determination of the spatial pattern of a lateral pressure head profile, corresponding to any given lateral slope, involves a hydraulic simulation. By comparison, the simulation results presented here suggest that given slope the corresponding lateral pressure head profile pattern can be determined simply by comparing the lateral slope with a pair of threshold slopes that are unique to the lateral. Evidently, this will simplify the process by which the spatial patterns of lateral pressure profiles are determined, as a function of slope, and enhances the practical utility of the results of the theoretical analysis. However, results of the simulation study are essentially empirical and as such applicable only to the data sets considered here. Thus, comprehensive simulation studies might be needed to conclusively establish the broader practical significance of these results.

Pressure Head Profile Pattern Categories

Theoretical analysis of slope effects on lateral pressure head profile patterns is presented in the companion manuscript. The analysis assumes that the hydraulic, geometric, and slope parameter set of a lateral constitutes a feasible hydraulic scenario and is spatially invariant. The key inferences deduced in the companion paper are reproduced here for convenience:

(1) The spatial pattern of the pressure head profile of a lateral, and possibly the locations of the pressure head extrema along the lateral, can be determined by simply comparing the negative of the lateral slope, $-\psi_i$, with the corresponding friction slopes at the upstream, $H_f'(0,\psi_i)$, and/or distal, $H_f'(l,\psi_i)$, ends of the profile and

(2) The full range of variation of the pressure head profile patterns of a lateral consist of three distinct categories (described as category *I*, *II*, and *III*), provided the lateral slope can be varied over a sufficiently wide range.

The characteristic features of the pressure head profile pattern categories are:

(1) if the negative of the lateral slope equals or exceeds the maximum of the corresponding friction slope profile (which is located at the lateral inlet), then the results show the pressure head profile is a monotonic increasing function of distance from inlet and such a spatial pattern is labeled here as category *I*;

(2) if the negative of a lateral slope is within the range of variation of the corresponding friction slope profile, the results of the analysis show that the pressure head profile should have two segments, consisting of a decreasing upstream and an increasing downstream section with a minimum pressure head somewhere in between the inlet and distal ends, and the spatial pattern of such a profile is described here as category *II*; and

(3) if the minimum of the friction slope profile of a lateral (which occurs at the distal end) equals or exceeds the negative of the corresponding lateral slope, then the pressure head profile is a decreasing function of distance from inlet and is defined here as category *III* pattern.

A summary of the properties of the pressure head profile pattern categories and the locations of the pressure head extrema along a lateral is presented in the companion paper and is reproduced here for convenience in Table 1.

Friction Slope and Pressure Slope Profiles and Lateral Threshold Slopes

The friction slope, $H_f'(x,\psi_i)$, at the upstream and distal ends of a lateral and the pressure slope profile, $h'(x,\psi_i)$, of the lateral are important parameters in the characterization of pressure head profile patterns. Thus, equations for calculating the $H_f'(x,\psi_i)$ and $h'(x,\psi_i)$ profiles from simulated friction head loss and pressure head profiles are presented here.

Friction slope profile

As shown in the companion paper, friction slope, $H_f'(x,\psi_i)$, is a step function of distance from inlet and is defined over each lateral pipe segment (i.e., sprinkler spacing). However, in the current study it is approximated with a continuous function. With the continuous approximation, the friction slope over a lateral pipe segment is represented by a point located at the upstream end node of the segment. Then, the curve connecting these points, which is a monotonic decreasing function of distance from inlet, is used as a continuous approximation of the friction slope profile. Accordingly, the friction slope at a computational node along a lateral, say at distance x_q from lateral inlet, $H_f'(x_q,\psi_i)$, is calculated with the expression

$$H_f'(x_q,\psi_i) = \frac{H_f(x_q+\Delta x,\psi_i) - H_f(x_q,\psi_i)}{\Delta x}$$

In eqn. (1), $H_f(x_q,\psi_i)$ is the friction head loss in a section of the lateral that extends over a distance of x_q from the lateral inlet, for a lateral slope of ψ_i *[L]*; x_q is the distance of the *qth* computational node

	Lateral slope ranges					
	ψ_l<0					***ψ_l ≥ 0***
Relationships between ψ_l and H_f' at the inlet and/or distal ends of the profile	$-\psi_l>H_f'(0,\psi_l)$	$-\psi_l=H_f'(0,\psi_l)$	$H_f'(l,\psi_l)<-\psi_l<H_f'(0,\psi_l)$	$-\psi_l=H_f'(l,\psi_l)$	$0<-\psi_l<H_f'(l,\psi_l)$	$-\psi_l<H_f'(l,\psi_l)$
Scenarios[a]	*Scenario iia*	*Scenario iib*	*Scenario iic*	*Scenario iid*	*Scenario iie*	*Scenario i*
Pressure head, *h*, profile pattern[b]	*Increasing, $(h'(x,\psi_l)>0$ for $x\in[0,l])$*	*Increasing, $(h'(x,\psi_l)=0$, for x=0 and $h'(x,\psi_l)>0$, for $x\in(0,l]$)*	*Decreasing/Increasing[c], $(h'(x,\psi_l)<0$, for $x\in[0,x_{min})$, $h'(x,\psi_l)=0$, for $x=x_{min}$, and $h'(x,\psi_l)>0$, for $x\in(x_{min}, l])$*	*Decreasing, $(h'(x,\psi_l)<0$, for $x\in[0,l)$ and $h'(x,\psi_l)=0$, for x=l)*	*Decreasing, $(h'(x,\psi_l)<0$ for $x\in[0,l])$*	
Location of minimum *h*	*Inlet end*	*Inlet end*	*$(0<x_{min}<l)$[d]*	*Distal end*	*Distal end*	
Location of maximum *h*	*Distal end*	*Distal end*	*Inlet/distal end[e]*	*Inlet end*	*Inlet end*	
Categories [f]	*I*		*II*	*III*		

[a] Scenarios defined in the companion paper based on relationships between lateral and friction slopes;
[b] The spatial patterns of lateral pressure head profiles are described as *Increasing* and *Decreasing*. The term *Increasing* implies that the lateral pressure head profile increases with distance from inlet and the converse is true for those profile categories labeled as *Decreasing*;
[c] The lateral pressure head profile consists of a decreasing upstream segment and an increasing downstream segment;
[d] The minimum pressure head occurs somewhere in between the inlet and distal ends of the lateral, its exact location varies depending on the lateral slope, specific discussion on this is provided in the companion paper;
[e] The maximum pressure head occurs at the inlet and/or distal end of the lateral;
[f] Categories of pressure head profile patterns;

Table 1: Lateral pressure head profile pattern categories.

from the lateral inlet *[L]*; $q=0$ at the lateral inlet and increases along the lateral; Δx is the computational interval used in hydraulic simulation of irrigation laterals *[L]* and is the same as the sprinkler spacing.

Pressure slope profile

Pressure slope profile as well is a step function of distance from lateral inlet, but it is represented here as a continuous function. Following the same approach as that used for friction slope the pressure slope at a computational node, say at distance x_q from lateral inlet, $h'(x_q,\psi_i)$, is calculated with the expression

$$h'(x_q,\psi_i)=\frac{h(x_q+\Delta x,\psi_i)-h(x_q,\psi_i)}{\Delta x} \quad (2)$$

In eqn. (2), the pressure slope at a computational node is given as the pressure slope over the lateral pipe segment just downstream of the node. As shown in the companion paper, the pressure slope profile, $h'(x_q,\psi_i)$, can be calculated with

$$h'(x,\psi_i)=-\psi_i-H_f'(x,\psi_i) \quad (3)$$

However, the pressure slope profile, h', is calculated here independently with eq. 2. The implication is that h' calculated with eqn. (2) should be in agreement with that obtained with eqn. (3). Further discussion on this will be presented shortly.

Computation of lateral threshold slopes

The relationships between lateral slope and the corresponding friction slopes at the inlet and distal ends of the lateral are key to determining the pressure head profile pattern of a lateral with a given hydraulic and geometric parameter set. A close look at the results of the analysis presented in the companion paper show that there are two types of slopes, labeled here ψ_l and ψ_u, that satisfy the requirements

$$h'(0,\psi_i)=0, \quad hence \quad -\psi_i=H_f'(0,\psi_i) \quad for \quad \psi_i=\psi_l \quad (4)$$

at the lateral inlet and

$$h'(l,\psi_i)=0, \quad hence \quad -\psi_i=H_f'(l,\psi_i), \quad for \quad \psi_i=\psi_u \quad (5)$$

at the distal end of the h' and H_f' profiles. Eqn. (4) states that if ψ_l is a lateral slope for which the pressure slope at the inlet, $h'(0,\psi_l)$, is zero, it then follows from the pressure slope equation, Eq. 3, that $-\psi_l=H_f'(0,\psi_l)$. Likewise, eqn. (5) shows that if $h'(l,\psi_u)=0$, it can then be shown that $-\psi_u=H_f'(l,\psi_u)$. It will be shown shortly that these slopes (ψ_l and ψ_u) are important constants in the differentiation of lateral pressure head profile patterns into distinct categories. ψ_l and ψ_u will, henceforth, be referred to as the lower and upper lateral threshold slopes, respectively. Note that the threshold slopes cannot be expressed as explicit functions of friction and pressure slopes, thus they need to be computed iteratively such that some preset error tolerance labeled here as, ε, is satisfied. Accordingly, ψ_l can be computed with the following conditions in force

$$\left|h'(0,\psi_l)\right|\le\varepsilon \quad and \quad \left|-\psi_i-H_f'(0,\psi_l)\right|\le\varepsilon \quad (6)$$

and ψ_u can be determined such that

$$\left|h'(l,\psi_u)\right|\le\varepsilon \quad and \quad \left|-\psi_i-H_f'(l,\psi_u)\right|\le\varepsilon \quad (7)$$

Note that for the current application ψ_l and ψ_u are computed through trial and error such that eqns. (6) and (7) are satisfied within a tolerance of 0.005%. As can be noted from eqns. (4) and (5), the satisfaction of the error tolerance criteria for h', in both eqns. (6) and (7), should automatically imply that the absolute differences between the corresponding $-\psi_u$ and H_f' are satisfied. However, in acknowledgement of the fact that h' and H_f' are determined based on numerical simulations, the simultaneous satisfaction of the error tolerance criteria for both h' and the absolute difference between the corresponding $-\psi_u$ and H_f' is sought here in computing the approximate values of ψ_l and ψ_u.

Description of the Simulation Study and Data

The relationships between lateral slopes and pressure head profile patterns, predicted by the results of the analysis presented in the companion paper, were evaluated here based on results of simulations. Accordingly, hydraulic simulations were conducted with a numerical model developed by Zerihun and Sanchez (6). The simulations were based on three different data sets, covering a wide range of spatially invariant lateral hydraulic and geometric characteristics (Table 2). For each data set, nineteen different simulations were conducted keeping all other factors constant except lateral slopes. Lateral slopes were varied in

the ranges -8.5 and 2.5% for data set 1, -2.5 and 1.0% for data set 2, and -1.25 and 0.5% for data set 3. However, for clarity of presentation the results presented here are limited to only eleven different lateral slopes per data set. Note that for each data set lateral slopes were varied over a sufficiently wide interval so that the full range of variation of lateral pressure head profile patterns is covered. Results of the simulation study are presented in the following sections.

Characterization of Pressure Slope and Pressure Head Profiles Based on the Relationship Between $-\psi_i$ and $H_f'(x,\psi_i)$: Data Set 1

Simulated profiles, of data set 1, corresponding to eleven different lateral slopes ranging between -8.5 and 2.5% are shown in Figure 1. Figure 1a depicts $-\psi_i$ profiles superimposed on the corresponding friction slope profiles, $H_f'(x,\psi_i)$. Furthermore, the pressure slope, $h'(x,\psi_i)$, and the pressure head, $h(x,\psi_i)$, profiles of data set 1 are shown in Figures 1b and 1c, respectively.

Lateral variables/parameters	Units	Data sets		
		1	2	3
Sprinkler spacing	*m*	9.14	9.14	9.14
Coefficient of sprinkler pressure head-discharge function, ρ,	*(L/s) (1/m)$^{\lambda}$*	0.0125	0.0185	0.0258
Exponent of sprinkler pressure head-discharge function, λ,	-	0.520	0.515	0.502
Lateral diameter	*mm*	50.8	76.2	101.6
Lateral length	*m*	274.2	365.6	457.0
Lateral slope	*%*	[-8.5,2.5]	[-2.5,1.0]	[-1.25,0.5]
Lateral pipe absolute roughness	*mm*	0.508	0.254	0.127
Constant total head at the lateral inlet	*m*	55	45	35
Elevations at lateral inlet	*m*	25	25	17
Note: It is the range of variation of the lateral slope and not the exact values that are indicated in the table. Slope is invariant along a lateral, but for each data set simulations were conducted with different lateral slopes that span the indicated ranges.				

Table 2: Data used in lateral hydraulic simulations.

For convenience, discussion of the results obtained for each data set is organized in accordance with the following format. First, the pressure head profile pattern corresponding to lateral slopes that satisfy the criterion $-\psi_i \geq H_f'(0,\psi_i)$ [i.e., category *I* pattern] will be discussed (Table 1). This is followed by analysis of the profile pattern related to lateral slopes that meet the criterion $-\psi_i \leq H_f'(l,\psi_i)$ [i.e., category *III* pattern]. The discussion on the pressure head profile pattern corresponding to lateral slopes that satisfy the criterion $H_f'(l,\psi_i)<-\psi_i<H_f'(0,\psi_i)$ [i.e., category *II* pattern] will then be presented based on the results obtained for category *I* and *III* patterns.

Lateral slopes that satisfy the criterion $-\psi_i \geq H_f'(0,\psi_i)$

The discussion here follows the following sequence. First, the horizontal $-\psi_i$ lines in Figure 1a will be compared with the respective $H_f'(x,\psi_i)$ profiles. Results of the comparison between the $-\psi_i$ and $H_f'(x,\psi_i)$ profiles coupled with the results of the theoretical analysis, presented in the companion paper, will be used to predict the behaviors of the corresponding $h'(x,\psi_i)$ and $h(x,\psi_i)$ profiles. The simulated $h'(x,\psi_i)$ and $h(x,\psi_i)$ profiles, depicted in Figures 1b and 1c, will then be used to verify those observations.

Comparisons of $-\psi_i$ and friction slope, $H_f'(x,\psi_i)$, profiles: Note that in Figure 1a, it is $-\psi_i$, instead of ψ_i, that is shown on the vertical axis alongside $H_f'(x,\psi_i)$. Thus, it is important to observe here that as $-\psi_i$ increases, lateral slope, ψ_i, decreases. As can be noted from Figure 1a,

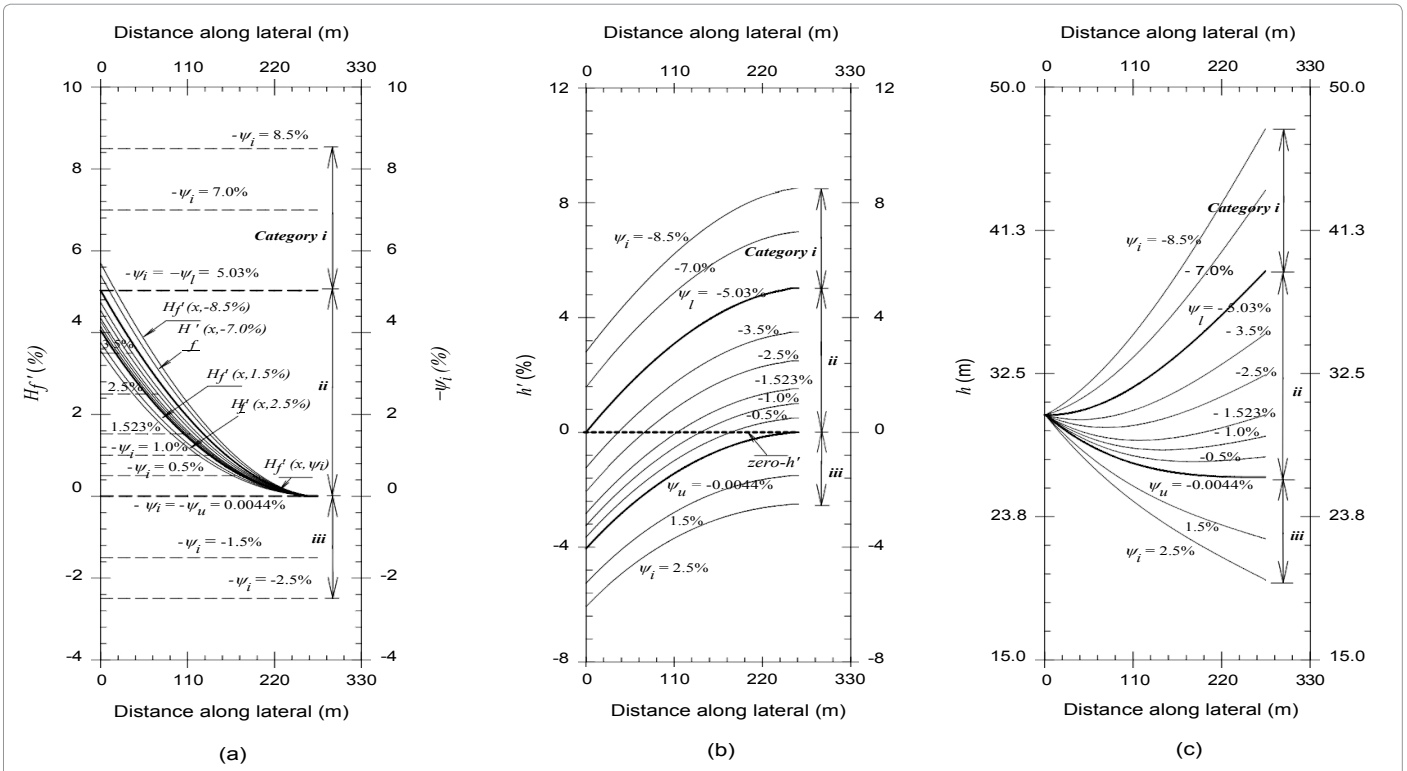

Figure 1: Simulated friction slope, $H_f'(x,\psi)$, pressure slope, $h'(x,\psi)$, and pressure head, $h(x,\psi)$, profiles of data set 1, for eleven different lateral slopes, ψ_i, ranging between a minimum of -8.5% and a maximum of 2.5%: (a) Friction slope profiles, $H_f'(x,\psi)$, superimposed on the corresponding $-\psi_i$ profiles, (b) Pressure slope profiles, $h'(x,\psi)$, and (c) Pressure head profiles, $h(x,\psi)$.

for any given lateral slope the corresponding $-\psi_i$ profile consists of a horizontal line. By contrast, the friction slope profiles, $H_f'(x,\psi_i)$, are decreasing convex functions of distance from the lateral inlet. Note that this observation is consistent with the general spatial behavior of $H_f'(x,\psi_i)$ of an irrigation lateral with a spatially invariant parameter set. The $H_f'(x,\psi_i)$ curves show maximum degree of spread at the lateral inlet as lateral slope is varied. The curves then tend to converge toward a horizontal line, along which $H_f'(x,\psi_i)=0$, as distance from lateral inlet increases. Furthermore, Figure 1a shows that the friction slope profiles appear to have intersected at or near the distal end of the laterals. However, this is because of scale effects. A closer look at the data shows that actually the friction slope profiles, $H_f'(x,\psi_i)$, are uniquely related to lateral slopes, ψ_i, and that at any given point along the lateral friction slope is a decreasing function of lateral slope (i.e., $H_f'(x,\psi_i)$ shows a downward shift as lateral slope increases). Now the $-\psi_i$ and $H_f'(x,\psi_i)$ profiles depicted in Figure 1a and their relationship with the corresponding $h'(x,\psi_i)$ and $h(x,\psi_i)$ profiles will be discussed.

Considering the lateral slope at the lower end of the slope range of data set 1 (which is -8.5%), it can be observed that the corresponding $-\psi_i$ profile, which is invariant with distance from the lateral inlet, is 8.5% (Figure 1a). The maximum of the corresponding friction slope profile which occurs at the inlet, $H_f'(0,-8.5\%)$, is 5.69%. Thus, for ψ_i=-8.5%, the $-\psi_i$ profile lies well above the friction slope curve, $H_f'(x,-8.5\%)$, over the entire lateral length [i.e., $-\psi_i > H_f'(x,\psi_i)$, for $0 \le x \le l$]. As ψ_i is increased from -8.5 to -7.0%, the corresponding H_f'curve shows a slight downward shift. The maximum of the friction slope profile for ψ_i=-7.0%, $H_f'(0,-7.0\%)$, is 5.41%. By contrast, the constant $-\psi_i$ profile is 7.0%. Although the $-\psi_i$ profile shows a significantly larger decrement than the maximum friction slope, $H_f'(0,\psi_i)$, as ψ_i is increased from -8.5 to -7.0%, the $-\psi_i$ profile still lies entirely above the $H_f'(x,-7.0\%)$ curve.

The results summarized above and additional simulated profiles (not depicted in Figure 1a for reason of clarity) suggest a trend in which both the $-\psi_i$ and $H_f'(x,\psi_i)$ profiles show a steady downward shift as lateral slope is increased, but $-\psi_i$ changes at a faster rate than the maximum change in $H_f'(x,\psi_i)$. The results also show that the $-\psi_i$ profiles lie entirely above the respective friction slope profiles, provided the lateral slope is less than -5.03%. For ψ_i=-5.03%, however, the absolute difference between $-\psi_i$ and the maximum friction slope, $H_f'(0,\psi_i)$, falls within the tolerance specified earlier in eqn. (6), which is 0.005%. Thus, results of the theoretical analysis suggest that for ψ_i=-5.03%, the lateral inlet should be a stationary point on the pressure head profile [i.e., $-\psi_i \approx H_f'(0,\psi_i)$ and $h'(0,\psi_i) \approx 0$] and hence -5.03% can be considered an approximation of the lower threshold slope, ψ_l, for data set 1. As can be noted from Figure 1a, the corresponding $-\psi_i$ and H_f' profiles show that $H_f'(x,-5.03\%) \approx 5.03\%$ at $x=0$ and $5.03\% > H_f'(x,-5.03\%)$ for $x>0$. Note that the $-\psi_l$ and $H_f'(x,\psi_l)$ profiles are shown in Figure 1a with heavier lines to indicate the significance of ψ_l as a threshold slope.

The results presented above imply that in the slope subinterval [-8.5%,-5.03%], which is a subset of the interval $\psi_i \le \psi_l$ (i.e., $\psi_i \le -5.03\%$), $-\psi_i$ exceeds the corresponding friction slope over the entire lateral length, except in the scenario where $\psi_i=\psi_l$ and hence $-\psi_i \approx H_f'(0,\psi_i)$. Specifically, this shows that $-\psi_i > H_f'(0,-5.03\%)$ for ψ_i<-5.03% and $-\psi_i \approx H_f'(0,\psi_i)$ for ψ_i=-5.03%. Thus, based on the results of the analysis presented in the companion paper, it can be observed that for each ψ_i in the slope subinterval [-8.5%,-5.03%], the corresponding pressure slope profile, $h'(x,\psi_i)$, should be greater than zero over the entire lateral length, except at the inlet where it would be sufficiently close to zero if $\psi_i=\psi_l$. This shows that the respective pressure head profiles should be increasing functions of distance from the inlet and hence the profile pattern should be category *I* (Table 1). These observations will now be verified based on the pressure slope and pressure head profiles depicted in Figures 1b and 1c.

Pressure slope, $h'(x,\psi_i)$, and pressure head, $h(x,\psi_i)$, profiles: Figure 1b depicts the pressure slope profiles, $h'(x,\psi_i)$, computed with eqn. (2) for eleven lateral slopes that vary in the interval -8.5% to 2.5%. Note that for each pressure slope profile, the $h'(x,\psi_i)$ computed with eqn. (2) were compared with those obtained with eqn. (3) and they all agree within a tolerance of 0.2% or less. The pressure slope profile for each ψ_i is an increasing function of distance from lateral inlet. However, a more useful perspective, for characterization of the spatial patterns of lateral pressure head profiles, consists of one in which the $h'(x,\psi_i)$ profiles are compared with the zero-h' line. The zero-h' line is a horizontal line along which the pressure slope of the lateral is zero. It can be observed from Figure 1b that based on the relative positions of the pressure slope profiles with respect to the zero -h' line three distinct types of pressure slope profiles, $h'(x,\psi_i)$, can be discerned. These include profiles that are completely above or below the zero-h' line and those profiles that have a segment above and another segment below the zero -h' line. These behaviors of the pressure slope profiles will now be related to the observations made earlier based on $-\psi_i$ and $H_f'(x,\psi_i)$.

As can be noted from Figure 1b, the pressure slope profiles for ψ_i=-8.5 and -7.0% lie entirely above the zero-h' line (Figure 1b), thus, $h'(x,\psi_i)>0$ for $0 \le x \le l$. Furthermore, these results and additional simulations (not shown in Figure 1b) suggest a trend in which at any given point along the lateral, pressure slope steadily decreases as lateral slope increases (i.e., the pressure slope curves show a downward shift as lateral slope increases). The results also show that the pressure slope profiles remain positive over the entire length of the lateral provided the lateral slope is less than -5.03%. For ψ_i=-5.03%, however, the minimum of the corresponding pressure slope profile, which occurs at the lateral inlet, falls within the tolerance specified in eqn. (6). Accordingly, for ψ_i=-5.03% the inlet end of the lateral represents a stationary point on the corresponding pressure head profile curve [i.e., $h'(0,-5.03\%) \approx 0$)] and hence -5.03% is an approximation of the lower lateral threshold slope, ψ_l, for data set 1. Note that the corresponding pressure slope profile, shown with a heavier solid line in Figure 1b, has the following properties: $h'(x,-5.03\%) \approx 0$ at $x=0$ and $h'(x,-5.03\%)>0$, for $0<x \le l$. The results summarized here show that for lateral slopes that vary in the subinterval [-8.5%,-5.03%], the corresponding pressure slope profiles depicted in Figure 1b have the following behavior: $h'(x,\psi_i)$ exceeds zero over the entire lateral length, except at the inlet end where it would be zero if $\psi_i=\psi_l$. Note that these results are in agreement with the observations made earlier based on the relationships between $-\psi_i$ and $H_f'(0,\psi_l)$.

Considering lateral slopes in the subinterval [-8.5%,-5.03%], which is a subset of the interval $\psi_i \le \psi_l$, a comparison of $-\psi_i$ with $H_f'(x,\psi_i)$ presented earlier (Figure 1a) and the behavior of the pressure slope profiles (Figures 1b) discussed above imply that the corresponding pressure head profiles should be increasing functions of distance from inlet. Accordingly, for each of these profiles the minimum and maximum pressure heads should occur at the inlet and distal ends of the profile, respectively, and the applicable profile pattern should be category *I* (Table 1). Note that for the slope subinterval -8.5% $\le \psi_i \le$ -5.03%, the spatial pattern of the profiles presented in Figure 1c is consistent with these observations.

Lateral slopes that satisfy the criterion $-\psi_i \le H_f'(l,\psi_i)$

The discussion here follows the same format as that used earlier in the scenario, where pressure profiles, corresponding to lateral

slopes that satisfy the criterion $-\psi_i \geq H_f'(l,\psi_i)$ were described. First, the horizontal $-\psi_i$ profiles, in Figure 1a, will be compared with the respective $H_f'(x,\psi_i)$ profiles. Results of the comparison coupled with those of the theoretical analysis will be used to predict the behaviors of the corresponding $h'(x,\psi_i)$ and $h(x,\psi_i)$ profiles. The simulated $h'(x,\psi_i)$ and $h(x,\psi_i)$ profiles, depicted in Figures 1b and 1c, will then be used to verify those observations.

Comparisons of $-\psi_i$ and friction slope, $H_f'(x,\psi_i)$, profiles: Now consider the lateral slope at the upper end of the slope range for data set 1, which is 2.5%. For ψ_i=2.5%, the constant $-\psi_i$ profile is -2.5% and the minimum of the friction slope profile which occurs at the distal end, $H_f'(l,2.5\%)$, is 0.0038% (Figure 1a). Thus, the $-\psi_i$ profile for ψ_i=2.5% lies well below the corresponding friction slope profile, $H_f'(x,2.5\%)$, over the entire length of the lateral (Figure 1a). As ψ_i is decreased from 2.5 to 1.5%, the H_f' profile shows a slight upward shift and as a result the minimum of the simulated friction slope profile for ψ_i=1.5%, $H_f'(l,1.5\%)$, increases from 0.0038% to 0.004%. On the other hand, the $-\psi_i$ profile, which is invariant with distance, is -1.5% and lies well below the corresponding $H_f'(x,1.5\%)$ over the entire length of the lateral.

The results presented here and additional results not depicted in Figure 1a, for clarity of presentation, suggest a trend in which both the constant $-\psi_i$ and the corresponding $H_f'(x,\psi_i)$ profiles show a steady upward shift as lateral slope decreases, however, the rate of change in $-\psi_i$ exceeds the maximum rate of change in the corresponding $H_f'(x,\psi_i)$. The results also show that the $-\psi_i$ lines remain entirely below the minimum of the corresponding $H_f'(x,\psi_i)$ profiles (which occur at the distal end), provided the lateral slope is greater than -0.0044%. For ψ_i=-0.0044%, however, the absolute difference between $-\psi_i$ and the minimum of the corresponding friction slope profile falls within the error tolerance specified in eqn. (7), which is 0.005%. Thus, for ψ_i=-0.0044%, the distal end of the lateral pressure head profile should be a stationary point [i.e., $-\psi_i \approx H_f'(l,\psi_i)$ and $h'(l,\psi_i) \approx 0$)] and hence -0.0044% can be considered as an approximation of ψ_u for data set 1. The corresponding $-\psi_u$ and $H_f'(x,\psi_u)$ profiles, depicted in heavier lines in Figure 1a, show that $H_f'(x,-0.0044\%) \approx 0.0044\%$ at $x=l$ and $-\psi_i < H_f'(x,-0.0044\%)$ for $0 \leq x < l$.

The results presented above suggest that in the slope subinterval [-0.0044%, 2.5%], which is the subset of the interval $\psi_i \geq \psi_u$ (i.e., $\psi_i \geq$ -0.0044%), $H_f'(x,\psi_i)$ exceeds $-\psi_i$ over the entire length of the lateral, except in the scenario where $\psi_i=\psi_u$ and hence $-\psi_i \approx H_f'(l,\psi_i)$. This implies that $-\psi_i < H_f'(l,-0.0044\%)$ for ψ_i>-0.0044% and $-\psi_i \approx H_f'(l,\psi_i)$ for ψ_i=-0.0044%. Results of the analysis presented in the companion paper, thus, suggest that for each ψ_i in the subinterval [-0.0044%,2.5%], the corresponding pressure slope profile, $h'(x,\psi_i)$, should be less than zero over the entire lateral length, except at the distal end where it would be sufficiently close to zero if $\psi_i=\psi_u$ (Table 1). It then follows that the corresponding pressure head profiles, $h(x,\psi_i)$, should be of category *III* pattern (Table 1). These observations will now be evaluated in light of the simulated pressure slope and pressure head profiles (Figures 1b and 1c).

Pressure slope, $h'(x,\psi_i)$, and pressure head, $h(x,\psi_i)$, profiles: Figure 1b shows that the pressure slope profiles for ψ_i=1.5 and 2.5% fall entirely under the zero-h' line, thus $h'(x,\psi_i)<0$ for $0 \leq x \leq l$. These as well as additional profiles not shown in Figure 1b suggest a trend in which the pressure slope profiles, $h'(x,\psi_i)$, show a steady upward shift as lateral slope, ψ_i, decreases. The results also show that the pressure slope profiles, $h'(x,\psi_i)$, remain negative over the entire lateral length, provided the lateral slope is greater than -0.0044%. For ψ_i=-0.0044% the maximum of the pressure slope profile (which is located at the distal end) falls within the error tolerance specified in eqn. (7). These results confirm the earlier observation that -0.0044% is an approximation of ψ_u for data set 1 and the distal end of the profile represents a stationary point on the corresponding pressure head profile [i.e., $h'(l,\psi_u) \approx 0$)]. For ψ_u=-0.0044%, the corresponding pressure slope, depicted with a heavier solid line in Figure 1b, shows that $h'(x,-0.0044\%) \approx 0$ at $x=l$ and $h'(x,-0.0044\%)<0$ for $0 \leq x < l$. The results summarized here suggest that in the slope subinterval [-0.0044%, 2.5%], the pressure slope profile is negative [i.e., $h'(x,\psi_i)<0$] over the entire lateral length, except at the distal end where it would be sufficiently close to zero if $\psi_i=\psi_u$. Note that these results are consistent with the observations made earlier regarding the behavior of $h'(x,\psi_i)$ based on the relationships between $-\psi_i$ and $H_f'(x,\psi_i)$.

Considering the lateral slope subinterval [-0.0044%,2.5%], which is a subset of the interval $\psi_u \leq \psi_i$, the relationships between the $-\psi_i$ and H_f' profiles discussed earlier (Figure 1a) and the behavior of the h' profiles presented above (Figure 1b) imply that the corresponding pressure head profiles should be decreasing functions of distance from inlet. Thus, the maximum and minimum of the corresponding pressure head profiles should occur at the inlet and distal ends, respectively, and the corresponding profile pattern should be category *III*. Note that in the slope subinterval $-0.0044\% \leq \psi_i \leq 2.5\%$, the spatial pattern of the simulated pressure head profiles depicted in Figure 1c is in agreement with these observations.

Lateral slopes that satisfy the criterion $H_f'(l,\psi_i)<-\psi_i<H_f'(0,\psi_i)$

Here as well, the presentation is organized following the same format as that used earlier in relation to the scenarios, where pressure profiles, corresponding to lateral slopes that satisfy the criteria $-\psi_i \geq H_f'(0,\psi_i)$ and $-\psi_i \leq H_f'(l,\psi_i)$ were discussed.

Comparisons of $-\psi_i$ and friction slope, $H_f'(x,\psi_i)$, profiles: A close look at Figure 1a shows that for data set 1, lateral slopes that satisfy the criterion $H_f'(l,\psi_i)<-\psi_i<H_f'(0,\psi_i)$ fall in the slope subinterval $\psi_l<\psi_i<\psi_u$ or $(-5.03\%,-0.0044\%)$. Note that in this slope subinterval five lateral slopes ranging between -3.5% and -0.5% are considered. For each ψ_i, the negative of the lateral slope profile intersects with the corresponding friction slope profile somewhere along the lateral, between the inlet and distal ends. In order to make the intersection points of a given pair of $-\psi_i$ and H_f' readily discernible from the others, for each ψ_i only a part of the $-\psi_i$ line that extends between the inlet end of the lateral and the point of intersection of the $-\psi_i$ with the corresponding H_f' are shown in Figure 1a. Note that the points of intersection of the horizontal $-\psi_i$ lines with the corresponding $H_f'(x,\psi_i)$ profiles represent the approximate locations, along the lateral, of the respective minimum pressure head points (i.e., stationary points at which $-\psi_i \approx H_f'(x_{min},\psi_i)$ and $h'(x_{min},\psi_i) \approx 0$).

Figure 1a shows that, for each ψ_i considered here, $H_f'(x,\psi_i)$ exceeds $-\psi_i$ over the interval $0 \leq x < x_{min}$ and thereafter $H_f'(x,\psi_i)$ falls below $-\psi_i$. The implication is that each of the corresponding pressure slope profiles, $h'(x,\psi_i)$, should have two segments: an upstream segment spanning the interval $0 \leq x < x_{min}$ where $h'(x,\psi_i)<0$ and a downstream segment extending over the interval $x_{min} < x \leq l$ with $h'(x,\psi_i)>0$. This in turn indicates that each of the respective pressure head profiles should have two segments as well: an upstream segment that decreases with distance from inlet and a downstream segment that increases with distance. These observations suggest that the pressure head profiles in this slope subinterval should be of category *II* pattern (Table 1). Furthermore, a close examination of Figure 1a shows that the distance of the minimum pressure head point from lateral inlet, x_{min}, is a strictly increasing function of lateral slope, ψ_i. The preceding observations can now be verified based on the pressure slope, $h'(x,\psi_i)$, and pressure head profiles, $h(x,\psi_i)$, (Figures 1b and 1c).

Pressure slope, $h'(x,\psi_i)$, and pressure head, $h(x,\psi_i)$, profiles: Considering lateral slopes in the interval *(-5.03%,-0.0044%)*, it can be observed from Figure 1b that each of the corresponding pressure slope profiles, $h'(x,\psi_i)$, intersects with the zero-h' line somewhere along the lateral between the inlet and distal ends. Evidently, the points of intersection of the zero-h' line with the pressure slope profiles, $h'(x,\psi_i)$, represent the approximate locations of the minimum pressure head points [i.e., $h'(x,\psi_i) \approx 0$] for the respective pressure head profiles. As can be noted from Figure 1b each of the pressure slope profiles has two segments: an upstream segment extending between the lateral inlet and the minimum pressure head point, over which $h'(x,\psi_i)<0$, and a downstream segment that spans the minimum pressure head point and the distal end of the lateral, in which $h'(x,\psi_i)>0$. Furthermore, it can be observed from Figure 1b that the zero-h' line intersects with the $h'(x,\psi_i)$ profiles at distances that increase with slope, which implies that x_{min} is an increasing function of ψ_i.

The results summarized above (Figure 1b) and those presented in an earlier discussion (Figure 1a) suggest that each of the corresponding pressure head profiles, $h(x,\psi_i)$, in the slope subinterval *(-5.03%,-0.0044%)* should have a decreasing upstream segment and an increasing downstream segment, with a minimum pressure head point somewhere along the lateral between the inlet and distal ends. The results also suggest that the maximum pressure head should occur at the inlet and/or distal ends of the lateral. Accordingly, the corresponding pressure head profile pattern should be of category *II*. Note that for lateral slopes that vary in the subinterval *(-5.03%,-0.0044%)*, the spatial pattern of the simulated pressure head profiles depicted in Figure 1c confirms the preceding observations.

It will be shown shortly that the x_{min} values determined based on the $h(x,\psi_i)$ profiles closely match those predicted based on a comparison of the $-\psi_i$ and $H_f'(x,\psi_i)$ curves (Figure 1a). A more detailed discussion of the relationships between lateral slope and lateral pressure head extrema and their locations along the lateral, in the slope subinterval $\psi_l<\psi_i<\psi_u$, will also be presented subsequently. Before that, however, simulation results for data sets 2 and 3 will be presented.

Characterization of Pressure Slope and Pressure Head Profiles Based on the Relationship Between $-\psi_i$ and $H_f'(x,\psi_i)$: Data Set 2

Figure 2 shows simulated profiles, of data set 2, corresponding to eleven lateral slopes varying between -2.5 and 1.0%. Figure 2a depicts the $-\psi_i$ profiles superimposed on the respective $H_f'(x,\psi_i)$ profiles. The corresponding pressure slope, $h'(x,\psi_i)$, and pressure head, $h(x,\psi_i)$, profiles are depicted in Figures 2b and 2c, respectively. Note that the $H_f'(x,\psi_i)$ profiles for data set 2 have the same mathematical properties as those noted in relation to the $H_f'(x,\psi_i)$ profiles of data set 1.

The simulation results presented earlier show that a pair of threshold slopes (ψ_l and ψ_u) can be computed for data set 1 based on the criteria set in Eqns. 6 and 7. The results also show that the threshold slopes delimit the slope range into three subintervals, each with a distinct pressure head profile pattern that corresponds to one of the categories summarized in Table 1. For data set 2, as well, approximations of the lower and upper threshold slopes were computed based on the requirements specified in Eqns. 6 and 7. Accordingly, the ψ_l and ψ_u values for data set 2 are -1.145 and -0.0011%, respectively. A closer look at Figures 2a-2c shows that the pair of slopes, ψ_l and ψ_u,

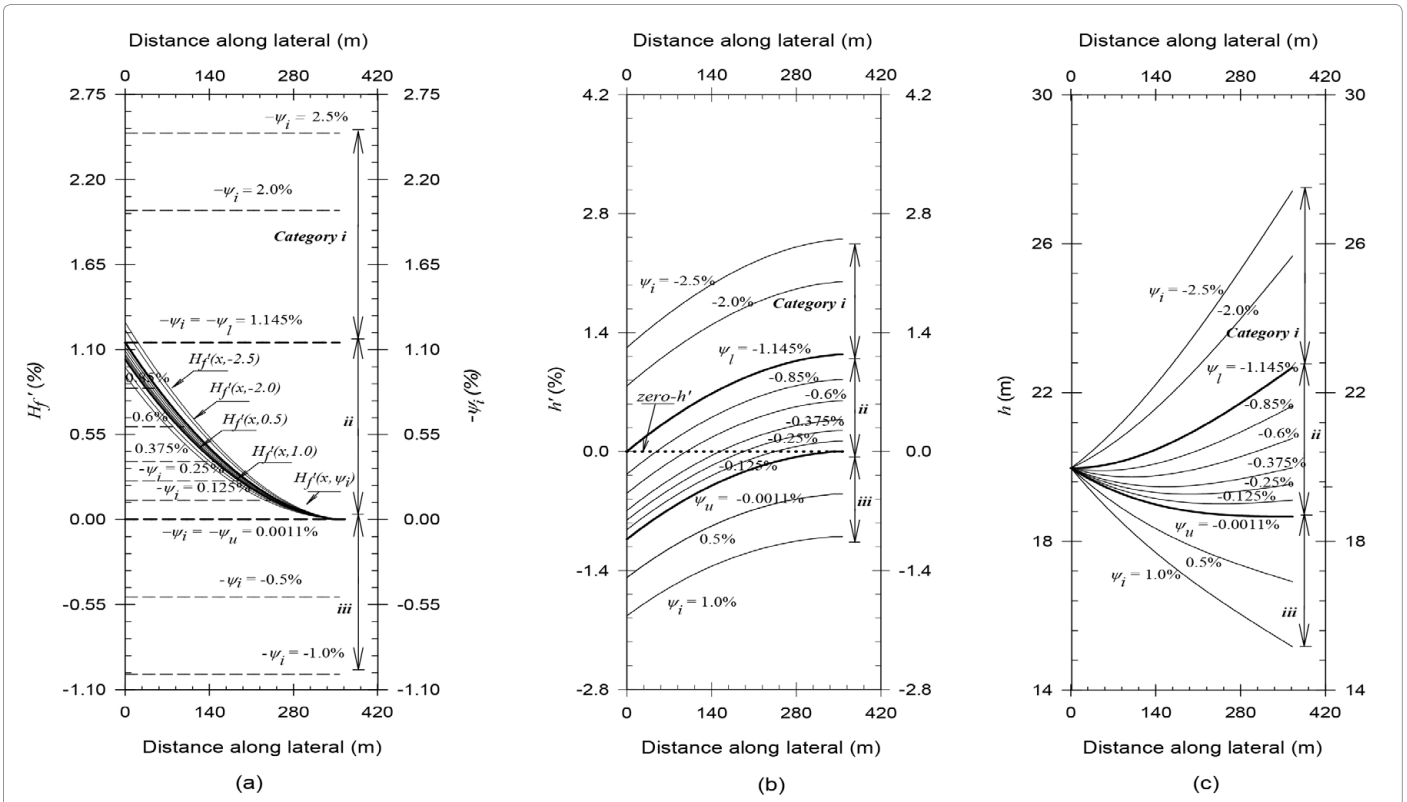

Figure 2: Simulated friction slope, $H_f'(x,\psi_i)$, pressure slope, $h'(x,\psi_i)$, and pressure head, $h(x,\psi_i)$, profiles of data set 2, for eleven different lateral slopes, ψ_i, ranging between a minimum of -2.5% and a maximum of 1.0%: (a) Friction slope profiles, $H_f'(x,)$, superimposed on the corresponding $-\psi_i$ profiles, (b) Pressure slope profiles, $h'(x,\psi_i)$, and (c) Pressure head profiles, $h(x,\psi_i)$.

delimit the lateral slope range, [-2.5%, 1.0%], into three subintervals: [-2.5%, -1.145%], (-1.145%,-0.0011%), and [-0.0011%, 1.0%], each with a distinct lateral pressure head profile pattern. Subsequent discussion will show that the spatial patterns of the lateral pressure head profiles in each these slope subintervals correspond to one of the pressure profile pattern categories deduced based on theory and summarized in Table 1. In order to indicate the significance of the threshold slopes in delimiting the lateral slope range into subintervals with distinct profile patterns, in Figure 2 the $-\psi_i$, $H_f'(x,\psi_i)$, $h'(x,\psi_i)$, and $h(x,\psi_i)$ profiles corresponding to ψ_l and ψ_u values are shown with heavier lines.

Lateral slopes that satisfy the criterion $-\psi_i \geq H_f'(0,\psi_i)$

First consider the lateral slope subinterval at the lower end of the slope range, [-2.5%,-1.145%], which is a subset of the interval $\psi_i \leq \psi_l$ (i.e., $\psi_i \leq$ -1.145%). Results summarized in Figure 2a and additional simulations not depicted here, for clarity, suggest that in this slope subinterval lateral slopes satisfy the criterion $-\psi_i > H_f'(x,\psi_i)$ over the entire length of the lateral, except in the scenario where $\psi_i=\psi_l$ and hence $-\psi_i \approx H_f'(0,\psi_i)$. Thus, based on the analysis presented in the companion paper it can be observed that the corresponding $h'(x,\psi_i)$ profiles should lie above the zero-h' line over the entire length of the lateral, except at the inlet end where it would be sufficiently close to zero if $\psi_i=\psi_l$ (Table 1). The implication is that, in this slope subinterval, the applicable $h(x,\psi_i)$ profile pattern should be category *I* and hence the minimum and maximum pressure heads should occur at the inlet and distal ends of the lateral, respectively. Note that the behaviors of the $h'(x,\psi_i)$ and $h(x,\psi_i)$ profiles in the slope subinterval -2.5 $\leq \psi_i \leq$ -1.145% (Figures 2b and 2c) are consistent with the observations made earlier based on the relationships between $-\psi_i$ and $H_f'(x,\psi_i)$.

Lateral slopes that satisfy the criterion $-\psi_i \leq H_f'(l,\psi_i)$

Now, consider lateral slopes at the upper end of the slope subinterval, [-0.0011%, 1.0%], which is a subset of the interval $\psi_i \geq \psi_u$ (i.e., $\psi_i \geq$ *-0.0011%*). The results presented in Figure 2a and additional simulations not depicted in Figure 2a, to enhance clarity of presentation, suggest that in this slope subinterval lateral slopes satisfy the criterion $-\psi_i < H_f'(l,\psi_i)$, except in the scenario where $\psi_i=\psi_u$ and hence $-\psi_i \approx H_f'(l,\psi_i)$. The theoretical analysis, thus, predicts that the corresponding pressure slope profiles should lie below the zero-h' line over the entire length of the lateral, except at the distal end where it would be zero if $\psi_i=\psi_u$ (Table 1). The implication is that, in the slope subinterval [-0.0011%, 1.0%], the $h(x,\psi_i)$ profiles should be of category *III* pattern and hence the maximum and minimum pressures should occur at the inlet and distal ends of the profiles, respectively. Note that the behaviors of the $h'(x,\psi_i)$ and $h(x,\psi_i)$ profiles in the slope subinterval [-0.0011%,1.0%], shown in Figures 2b and 2c, are in agreement with the observations made here based on the relationship between $-\psi_i$ and $H_f'(l,\psi_i)$.

Lateral slopes that satisfy the criterion $H_f'(l,\psi_i) < -\psi_i < H_f'(0,\psi_i)$

The results presented in Figure 2a show that the relationship, $H_f'(l,\psi_i) < -\psi_i < H_f'(0,\psi_i)$, should hold between ψ_i and H_f' in the slope subinterval $\psi_l < \psi_i < \psi_u$ or (-1.145%,-0.0011%). For each of the lateral slopes considered in this slope subinterval, the $-\psi_i$ profile intersects with the respective $H_f'(x,\psi_i)$ profiles somewhere along the lateral in between the inlet and distal ends. Evidently, the intersection points represent approximate locations, along the lateral, where pressure slopes should be zero and hence the corresponding pressure heads are the minimums of the respective profiles. Furthermore, Figure 2a shows that in the slope subinterval considered here the following relationship holds between $-\psi_i$ and $H_f'(x,\psi_i)$: $-\psi_i < H_f'(x,\psi_i)$ upstream of the minimum pressure head point and $-\psi_i > H_f'(x,\psi_i)$ downstream of the minimum pressure head point.

The preceding observations imply that, in this slope subinterval, $h'(x,\psi_i)<0$ over a section of the lateral that lies upstream of a minimum pressure head point and $h'(x,\psi_i)>0$ downstream of the minimum pressure head point. Thus, upstream of the respective minimum pressure head points, the pressure head profiles, $h(x,\psi_i)$, should be decreasing functions of distance from lateral inlet and downstream of the minimum pressure head points the pressure head profiles, $h(x,\psi_i)$, should be increasing functions of distance from the lateral inlet. Evidently, these observations imply that the maximum pressure head of each of the profiles, in the slope subinterval *(-1.145%,-0.0011%)*, should occur at the inlet and/or the distal ends. Accordingly, the spatial pattern of the pressure head profiles in this slope subinterval should be category *II*. Note that the behavior of the pertinent $h'(x,\psi_i)$ profiles shown in Figure 2b and the spatial patterns of the corresponding $h(x,\psi_i)$ profiles depicted in Figure 2c are in agreement with the observations made here based on the relationships between $-\psi_i$ and $H_f'(x,\psi_i)$.

Characterization of Pressure Slope and Pressure Head Profiles Based on the Relationship Between $-\psi_i$ and $H_f'(x,\psi_i)$: Data Set 3

Figure 3 shows simulated profiles, of data set 3, corresponding to eleven lateral slopes varying between -1.25 and 0.5%. The horizontal $-\psi_i$ lines superimposed on the corresponding $H_f'(x,\psi_i)$ profiles are depicted in Figure 3a. The pressure slope, $h'(x,\psi_i)$, and pressure head, $h(x,\psi_i)$, profiles for data set 3 are shown in Figures 3b and 3c, respectively.

The threshold slopes of data set 3 computed based on Eqns. 6 and 7 are ψ_l=-0.554% and ψ_u=-0.00037% (Figure 3a). Figures 3a-3c show that ψ_l and ψ_u delimit the lateral slope range, [-1.25%,0.5%], into three subintervals: [-1.25%,-0.554%], (-0.554%,-0.00037%), and [-0.00037%,0.5%], each with a distinct lateral pressure head profile pattern. It will be shown in subsequent discussion that each of these lateral slope subintervals correspond to one of the three pressure head profile patterns deduced based on theory and are summarized in Table 1. Note that in Figure 3, the $-\psi_i$, $H_f'(x,\psi_i)$, $h'(x,\psi_i)$, and $h(x,\psi_i)$ profiles corresponding to ψ_l and ψ_u values are shown with heavier lines so as to differentiate them from the rest of the profiles.

Lateral slopes that satisfy the criterion $-\psi_i \geq H_f'(0,\psi_i)$

First, consider the lateral slope subinterval at the lower end of the slope range, [-1.25%, -0.554%], which is a subset of the interval $\psi_i \leq \psi_l$ (i.e., $\psi_i \leq$ *-0.554%*). Results summarized in Figure 3a and additional simulations not depicted here, for clarity, suggest that in this slope subinterval lateral slopes satisfy the criterion $-\psi_i > H_f'(x,\psi_i)$ over the entire length of the lateral, except in the scenario where $\psi_i=\psi_l$ and hence $-\psi_i \approx H_f'(0,\psi_i)$. This implies that the corresponding pressure slope profiles, $h'(x,\psi_i)$, should be greater than zero over the entire length of the lateral, except at the inlet end where it would be zero if $\psi_i=\psi_l$. Thus, the applicable pressure head profile pattern should be category *I*. Note that the behaviors of the corresponding $h'(x,\psi_i)$ and $h(x,\psi_i)$ profiles presented in Figures 3b and 3c are consistent with the observations made here based on $-\psi_i$ and $H_f'(x,\psi_i)$.

Lateral slopes that satisfy the criterion $-\psi_i \leq H_f'(0,\psi_i)$

Now, consider lateral slopes at the upper end of the slope range, [-0.00037%, 0.5%], which is a subset of the interval $\psi_i \geq \psi_u$ ($\psi_i \geq$ *-0.00037%*). The results presented in Figure 3a and additional simulations not depicted here, for clarity, suggest that in this slope

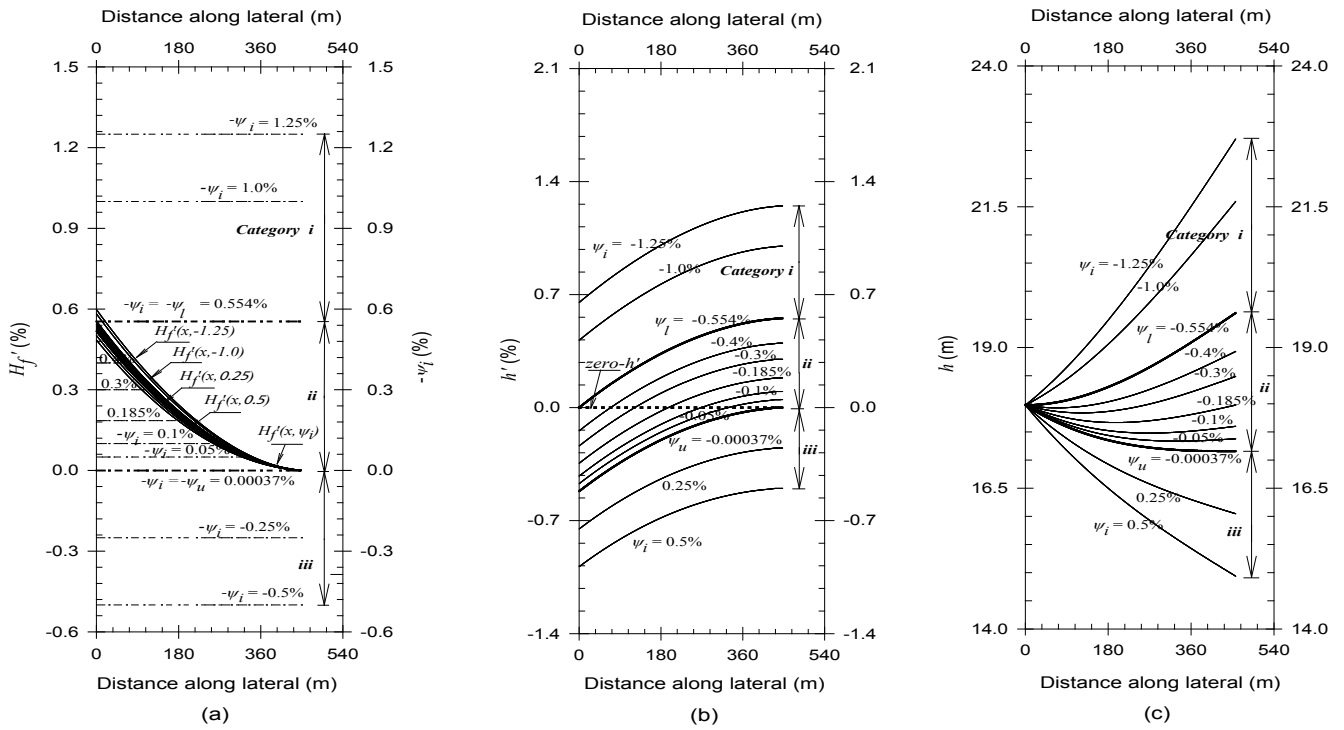

Figure 3: Simulated friction slope, $H_f'(x,\psi_i)$, pressure slope, $h'(x,\psi_i)$, and pressure head, $h(x,\psi_i)$, profiles of data set 3, for eleven different lateral slopes, ψ_i, ranging between a minimum of -1.25% and a maximum of 0.5%: (a) Friction slope profiles, $H_f'(x,\psi_i)$, superimposed on the corresponding $-\psi_i$ profiles, (b) Pressure slope profiles, $h'(x,\psi_i)$, and (c) Pressure head profiles, $h(x,\psi_i)$.

subinterval lateral slopes satisfy the criterion $-\psi_i<H_f'(l,\psi_i)$ over the entire length of the lateral, except in the scenario where $\psi_i=\psi_u$ and hence $-\psi_i \approx H_f'(l,\psi_i)$. This implies that $h'(x,\psi_i)$ should be less than zero over the entire lateral length, except at the distal end where it would be zero if $\psi_i=\psi_u$. Thus, the spatial pattern of the corresponding pressure head profiles should be category *III*. Note that the corresponding $h'(x,\psi_i)$ and $h(x,\psi_i)$ profiles shown in Figure 3b and 3c are in agreement with the preceding observations.

Lateral slopes that satisfy the criterion $H_f'(l,\psi_i)<-\psi_i<H_f'(0,\psi_i)$

The simulation results presented in Figure 3a show that the relationship, $H_f'(l,\psi_i)<-\psi_i<H_f'(0,\psi_i)$, holds between ψ_i and H_f' profiles in the slope subinterval $\psi_l<\psi_i<\psi_u$ or *(-0.554%,-0.00037%)*. Thus, for each ψ_i considered in this slope subinterval, a comparison of the $-\psi_i$ and H_f' profiles suggests that the corresponding pressure slope, $h'(x,\psi_i)$, should be zero somewhere along the lateral in between the inlet and distal ends, which represents the approximate location of the minimum pressure head point. The results summarized in Figure 3a also imply that in the section of the lateral that is upstream of the minimum pressure head point, $h'(x,\psi_i)$ should be less than zero and hence the corresponding $h(x,\psi_i)$ should be a decreasing function of distance from inlet. The results also indicate that downstream of the minimum pressure point, the $h'(x,\psi_i)$ profile should be greater than zero and hence the corresponding $h(x,\psi_i)$ profile should be an increasing function of distance from inlet. Evidently, these results suggest that the maximum pressure head of each of the profiles, in the slope subinterval *(-0.554%,-0.00037%)*, should occur at the inlet and/or the distal ends. The preceding, thus, implies that the applicable pressure head profile pattern should be category *II*. Note that the behavior of the pertinent $h'(x,\psi_i)$ profiles and the spatial pattern of the corresponding $h(x,\psi_i)$ profiles depicted in Figures 3b and 3c, respectively, are consistent with the observations made earlier based on the relationships between $-\psi_i$ and $H_f'(x,\psi_i)$.

A more detailed discussion of the relationships between lateral slopes and the lateral pressure head extrema and their locations along a lateral, in the slope subinterval $\psi_l<\psi_i<\psi_u$, will be presented next.

Lateral Pressure Head Extrema and Their Locations along A Lateral for Slopes That Vary in the Subinterval Delimited by the Lower and Upper Threshold Slopes

Introductory discussion

The simulation results presented in the preceding sections show that in the slope subintervals $\psi_{min} \le \psi_i \le \psi_l$ and $\psi_{max} \ge \psi_i \ge \psi_u$, the locations of the lateral pressure head extrema can be completely determined based on the spatial patterns of the lateral pressure head profiles (where ψ_{min} and ψ_{max} are the lower and upper limits, respectively, of the slope range of each of the data sets considered here). Note that this result is in agreement with the theoretical analysis. By comparison, in the slope subinterval $\psi_l<\psi_i<\psi_u$ (i.e., the interval in which the relationship $H_f'(l,\psi_i)<-\psi_i<H_f'(0,\psi_i)$ holds) the theoretical results do not provide an answer to the question of what are the exact locations of the minimum and maximum pressure head points along a lateral, given the lateral slope. The theoretical results only define the conditions for determining the location of the minimum pressure head point along a lateral, given a lateral slope, ψ_i. Furthermore, the theoretical results only indicate that the maximum pressure head point should be at the inlet and/or the distal ends, but do not provide specific criteria to determine the location either way, given a lateral slope. Thus, simulated pressure head profiles, shown in Figures 4a-4c, will be used here to gain some insight into the relationships between lateral slopes and lateral pressure head extrema and their locations along a lateral, in the subinterval $\psi_l<\psi_i<\psi_u$.

Note that the profiles in Figure 4 are extracted from those shown in Figures 1c, 2c, and 3c.

Relationships between minimum pressure head and lateral slope in the subinterval (ψ_l,ψ_u)

For each lateral pressure head profile, shown in Figure 4, a horizontal dotted line is used to mark the corresponding minimum pressure head on the vertical axis of the graph and a vertical dotted line marks the distance of the minimum pressure head point from the lateral inlet on the horizontal axis of the graph. In the subinterval $\psi_l<\psi_i<\psi_u$, the lateral pressure head profiles of each of the data sets show that the minimum pressure head and its location along the lateral follow a distinct pattern (Figures 4a-4c). As lateral slope is increased from ψ_l to ψ_u, for each data set the location of the minimum pressure head point steadily shifts downstream along the lateral from the upstream end (where $x_{min}=0$ for $\psi_i=\psi_l$) toward the distal end of the pressure head profile (where $x_{min}=l$ for $\psi_i=\psi_u$). Furthermore, the results also show that the minimums of the pressure head profiles decrease steadily as ψ_i increases (Figures 4a-4c). The peaks of the minimum pressure heads are 29.93, 19.97, and 17.98m for data sets 1, 2, and 3, respectively, and they occur at the inlet for $\psi_i=\psi_l$. The minimums of the pressure head profiles for data sets 1, 2, and 3 fall to their lowest levels of 26.13, 18.67, and 17.16m, respectively, at $\psi_i=\psi_u$ and they occur at the location of the penultimate sprinkler.

Note that the occurrence of the minimum pressure head at the penultimate sprinkler implies a positive pressure slope at the distal end lateral segment. This may appear to contradict the theoretical result, which requires that the pressure slope over the distal end lateral pipe segment to be zero when $\psi_i=\psi_u$. However, it is indicated in an earlier discussion that the pressure head profiles corresponding to $\psi_i=\psi_u$ are computed numerically such that the error tolerance requirements on $|h'|$ and $|-\psi_i-H_f'|$, specified in eqn. (7), are satisfied simultaneously. Thus, for each data set considered here these requirements were satisfied simultaneously when the pressure head profile in the distal end lateral pipe segment, takes a shallow but positive slope of 0.002% or less. Note that this explains the observed positive slope in the distal segment of the lateral. Evidently, the threshold slopes, ψ_l and ψ_u, are not within the slope subinterval considered here, which is (ψ_l,ψ_u). However, they are included in the current discussion, because they provide known boundary conditions with regard to the location of lateral pressure head extrema.

Relationships between maximum pressure head and lateral slope in the subinterval (ψ_l,ψ_u)

In contrast to the minimum pressure heads, the maximum pressure heads occur only at the inlet and/or the distal ends of the profiles and the variation of the maximum pressure heads with ψ_i follow a different pattern than that observed for the minimum lateral pressure heads. The peaks of the maximum lateral pressure heads are 38.74m for data set 1, 22.67 m for data set 2, and 19.62 m for data sets 3 and they occur at the downstream ends of the profiles and for $\psi_i=\psi_l$ (Figures 4a-4c). Now, as the lateral slope is increased steadily starting from ψ_l, for each data set the pressure head at the distal end, $h(l,\psi_i)$, decreases. Thus, increasing ψ_i starting from a lower limit of, ψ_l, initially leads to a decrease in the maximum lateral pressure head. However, unlike the minimum pressure head point, initially the location of the maximum pressure head remained at the downstream end of the profile.

By comparison, the pressure head at the opposite end of the lateral, $h(0,\psi_i)$, remained nearly constant at a level that closely approximates the difference between the total head and the lateral elevation at the inlet. As a result with further increases in ψ_i, a slope value, labeled here as ψ_τ, is reached for which the pressure head at the distal end falls to the same level as the pressure head at the upstream end of the profile. In which case, for $\psi_i=\psi_\tau$ the maximum pressure head occurs at both ends of the profile. However, as ψ_i is increased beyond ψ_τ the pressure head at the distal end falls below the pressure head at the upstream end and hence the location of the maximum pressure head shifts from the downstream end to

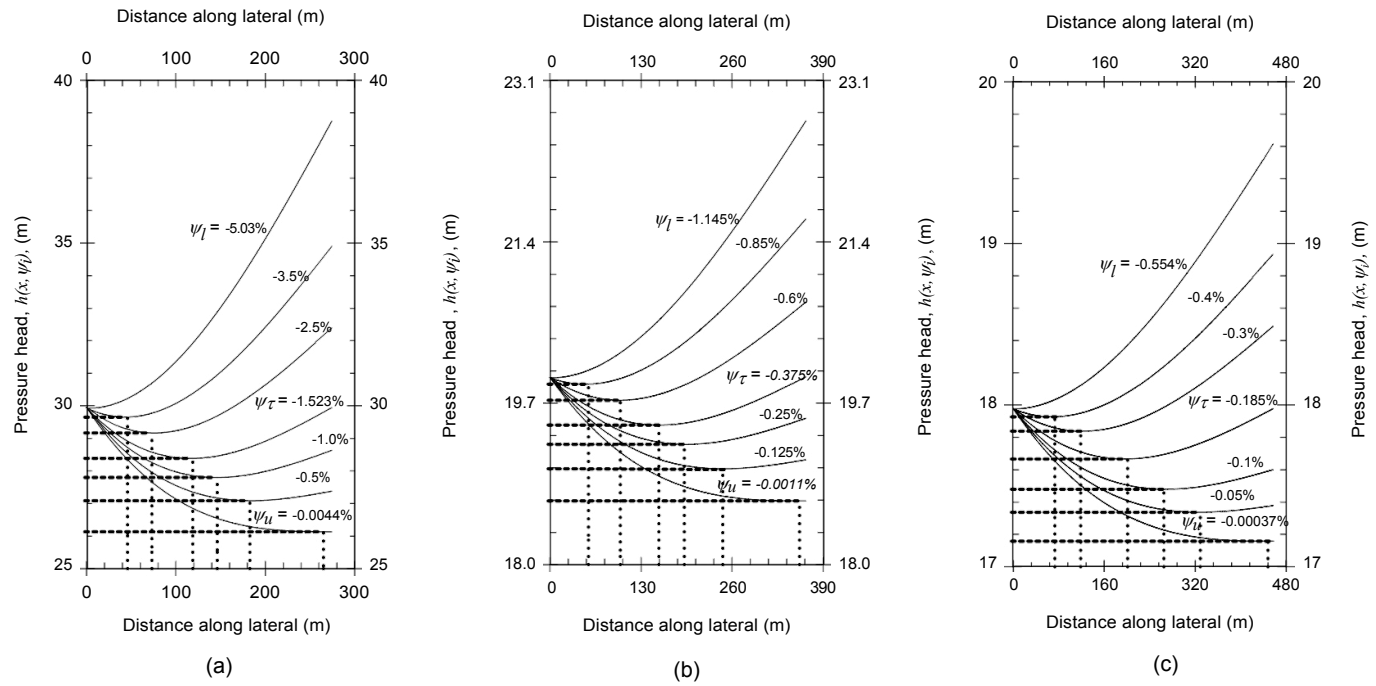

Figure 4: Simulated lateral pressure head profiles in the slope subinterval $[\psi_l,\psi_u]$: (a) data set 1, (b) data set 2, and (c) data set 3.

the upstream end of the profile and stays there as ψ_i approaches ψ_u.

Note that in the current application, for each data set ψ_τ is computed through trial and error such that the difference between the pressure heads at the two ends of a lateral is within a tolerance of 0.01 m. Approximate values of ψ_τ computed for data sets 1, 2, and 3 are -1.523, -0.375, and -0.185%, respectively (Figures 4a-4c). The corresponding maximum pressure heads are 29.94 for data set 1, 19.97 m for data set 2, and 17.97 m for data set 3. In the slope subinterval $[\psi_l,\psi_\tau)$, the maximum pressure head occurs at the distal end but decreases as lateral slope increases. Over the slope subinterval $(\psi_\tau,\psi_u]$, the maximum pressure head occurs at the lateral inlet and its value can be closely approximated by a constant head equal to the difference between the total head and the elevation of the lateral at the inlet, which is 30.0 m for data set 1, 20.0 m for data set 2, and 18.0 m for data set 3 (Figures 4a-4c). Note that the preceding results suggest that ψ_τ varies as a function of lateral hydraulic and geometric parameter set.

Comparison of Estimates of x_{min} Obtained from the Simulated Pressure Head Profiles with those Obtained Based on the Relationships between Lateral and Friction Slopes

Considering a lateral with a specified hydraulic and geometric parameter set and a lateral slope that varies in the subinterval $\psi_l<\psi_i<\psi_u$, the distance of the minimum pressure head point from lateral inlet, x_{min}, can be determined using one of two approaches. One option consists of determining x_{min} directly from the simulated lateral pressure head profile data, given a lateral slope, ψ_i. Alternatively, an estimate of x_{min}, given ψ_i, can be obtained through interpolation over the friction slope profile, such that the requirement $-\psi_i=H_f'(x,\psi_i)$ at $x=x_{min}$ is satisfied. Because of differences in the errors incurred in the determination of H_f and h profiles, estimates of x_{min} obtained with the alternative approaches can be slightly different. In addition, the continuous approximation of H_f' may also contribute to the differences in the x_{min} estimates of the alternative approaches.

As can be noted from Figures 4a-4c, for each data set there are five lateral slopes in the subinterval $\psi_l<\psi_i<\psi_u$. Comparison of the x_{min} estimates obtained with the alternative approaches, as a function of each ψ_i, are shown in 1:1 plots in Figures 5a-5c for data sets 1 to 3. Visual observation suggests that for all the data sets estimates of x_{min} obtained based on friction slope and lateral slope profiles are generally in good agreement with those determined based on the pressure head profile data. In order to obtain a quantitative measure of the differences between the predictions of the alternative approaches, the absolute residuals in the x_{min} determined with the two approaches, expressed as percentage of the x_{min} values obtained based on the pressure head profile data, are calculated. The maximum percent residuals between the x_{min} estimates obtained with the alternative approaches are 12.2, 11.0, and 5.2% for data sets 1, 2, and 3, respectively (Figures 5a-5c). The average percent residuals in the estimates of the distances of the minimum pressure head points from the lateral inlets are 4.1, 3.1, and 2.5%, for data sets 1, 2, and 3, respectively. The results show that the

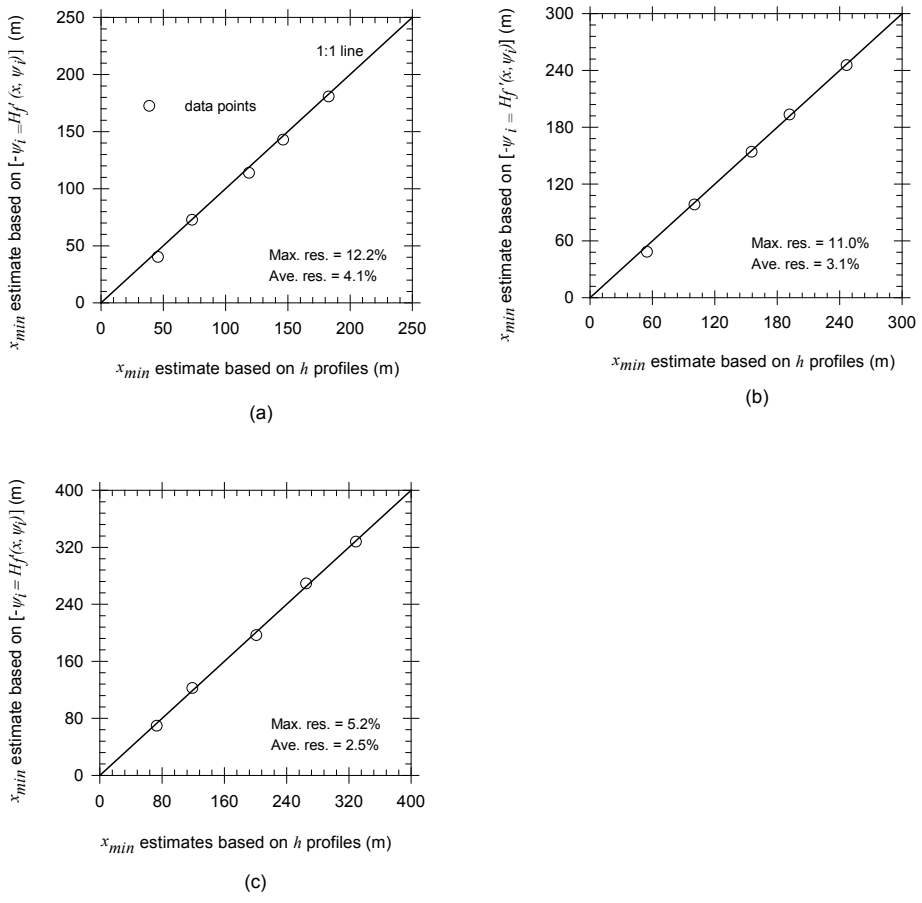

Figure 5: Comparison of estimates of x_{min} obtained from the simulated pressure head profiles with those obtained based on the relationships between lateral and friction slopes in the slope subinterval (ψ_l,ψ_u): (a) data set 1, (b) data set 2, and (c) data set 3.

maximum absolute difference between the estimates of x_{min} obtained with the alternative approaches is about 70% of the sprinkler spacing (or the computational interval used in the simulations).

Discussion

Verification of key results of the theoretical analysis

Results of the simulation study presented earlier show that, for each of the lateral slopes considered in the evaluation, a comparison of the negative of the lateral slope, $-\psi_i$, with the maximum, $H_f'(0,\psi_i)$, and/or minimum, $H_f'(l,\psi_i)$, of the corresponding friction slope profile can be used to determine the spatial pattern of the pressure head profile and possibly the locations of the pressure head extrema along the lateral. The results also show that the full range of variation of the spatial patterns of the pressure head profiles of each of the laterals considered here (i.e., data sets 1, 2, and 3) consists of three distinct categories: a profile pattern that is increasing or decreasing with respect to distance from inlet over the entire length of the lateral and one that combines both trends within the length of the lateral, labeled here as categories *I*, *II*, and *III* (Figures 1-3). This shows that the simulation results confirm the general inferences deduced in the companion paper based on theoretical analysis. Furthermore, the simulation results provide additional insights, of some practical significance, into the relationships between lateral slope and pressure head profile patterns. These results will be summarized subsequently.

A unique pair of lateral threshold slopes

The simulation study shows that for each of the data sets considered here there exists a unique pair of lateral slopes (ψ_l and ψ_u) that satisfy the requirements specified in Eqns. 4 and 5, although in practice only an approximation of them can be computed based on Eqns. 6 and 7. The computed threshold slopes are summarized here for convenience: ψ_l=-5.03% and ψ_u=-0.0044% for data set 1; ψ_l=-*1.145%* and ψ_u=-0.0011% for data set 2; and ψ_l=-0.554% and ψ_u=-0.00037% for data set 3. A couple of observations on the lateral threshold slopes may be in order here. Both the ψ_l and ψ_u values computed for each data set are less than zero. It ought to be noted here that this observation is not specific to the lateral parameter sets considered in the simulation study. In fact, it can be readily shown based on eqn. (3) that both ψ_l and ψ_u should be less than zero regardless of the parameters set. Furthermore, the results show that the upper lateral threshold slope is close to zero, while the lower threshold slope can differ from zero by a significant margin. The results also show that the threshold slopes can vary significantly depending on the lateral hydraulic and geometric parameter set. This empirical observation coupled with the fact that both ψ_l and ψ_u are related to $H_f'(x,\psi_i)$ through Eqns. 4 and 5, and that $H_f'(x,\psi_i)$ is in turn a function of the hydraulic and geometric parameter set of a lateral, implies that threshold slopes of a lateral as well are functions of the hydraulic and geometric parameter set of the lateral.

The threshold slopes delimit the slope range into subintervals each with a distinct lateral pressure head profile pattern

The results of the simulations show that for each data set the pair of threshold slopes delimit the range of variation of the lateral slope into well-defined subintervals, each with a distinct lateral pressure head profile pattern that corresponds to one of the three categories defined based on theory (Table 1). In the slope subinterval $\psi_{min} \le \psi_i \le \psi_l$, lateral slopes satisfy the criterion $-\psi_i \ge H_f'(l,\psi_i)$ and hence the corresponding lateral pressure head profiles are monotonic increasing functions of distance from inlet. Accordingly, the minimum and maximum pressure heads are located at the inlet and distal ends of the lateral, respectively, and the applicable profile pattern is category *I*. By comparison, in the subinterval $\psi_{max} \ge \psi_i \ge \psi_u$ lateral slopes satisfy the criterion $-\psi_i \le H_f'(l,\psi_i)$. It then follows that, in this slope subinterval, lateral pressure head profiles are decreasing functions of distance from lateral inlet and hence the maximum and minimum pressure heads are located at the inlet and distal ends, respectively. Accordingly, the pressure head profiles are of category *III* pattern.

The results also show that in the subinterval $\psi_l<\psi_i<\psi_u$, lateral slopes satisfy the criterion $H_f'(l,\psi_i)<-\psi_i<H_f'(0,\psi_i)$. A pressure head profile in this slope subinterval has two segments: a decreasing upstream and an increasing downstream segment with a minimum pressure head point somewhere along the lateral in between the inlet and distal ends. Thus, the corresponding pressure head profile pattern is category *II*. The essential results, for this slope subinterval, with regard to slope effects on pressure head extrema and their locations along the lateral are summarized here. The magnitude and location along the lateral of the pressure head extrema vary with the slope of the lateral. The minimum lateral pressure head decreases as lateral slope increases and the distance of the minimum pressure head point from the lateral inlet, x_{min}, is a strictly increasing function of lateral slope.

The results also suggest that for each data set considered here, there exists a lateral slope, ψ_τ, that delimits the slope subinterval (ψ_l,ψ_u) into two, (ψ_l,ψ_τ) and (ψ_τ,ψ_u), based on which the location of the maximum pressure head along the lateral can be determined. For $\psi_l<\psi_i<\psi_\tau$, the maximum pressure head occurs at the downstream end of the pressure head profile and decreases with ψ_i. For $\psi_i=\psi_\tau$, the pressure heads at the upstream and distal ends of the profile are equal, thus the maximum pressure head occurs at both ends of the profile. For $\psi_u>\psi_i>\psi_\tau$, the maximum pressure head occurs at the upstream end of the lateral and can be closely approximated by the difference between the total head at the lateral inlet and the elevation of the lateral inlet (thus in this slope subinterval the maximum pressure head is nearly constant).

Practical significance of the existence of a pair of threshold slopes unique to a lateral

As noted earlier, results of the theoretical analysis presented in the companion paper state that the spatial pattern of the pressure head profile of a lateral, given the lateral slope, can be determined by comparing the negative of the lateral slope with the corresponding friction slopes at the inlet and/or distal ends of the profile. However, the friction slope profile of a lateral is a function of the lateral slope. Thus, for any given lateral slope a complete hydraulic simulation needs to be conducted to ascertain the corresponding friction slope profile and hence the friction slopes at the inlet and distal ends. This implies that while the results of the theoretical analysis are generally true, they, however, produce particular solutions; i.e., solutions applicable only to the specific lateral slope. By contrast, results of the simulation study presented here suggest that the full range of variation of the pressure head profile patterns of a lateral can be completely determined as a function of a pair of threshold slopes that are unique to the lateral. The significance of this observation in terms of enhancing the practical utility of the results of the theoretical analysis will now be discussed.

Before proceeding further two important results of the simulation study will be tentatively generalized as follows: *(i)* For a lateral with a given spatially invariant hydraulic and geometric parameter set, there exists a unique pair of threshold slopes that delimits the feasible range of variation of the slope of a lateral into three subintervals, each with a particular pressure head profile pattern and *(ii)* the pressure head profile pattern of a lateral, within each of these slope subintervals, corresponds to one of the three categories defined based on theoretical analysis.

Based on these inferences, it can be readily reasoned that a complete characterization of all the possible pressure head profile patterns of a lateral requires only the iterative computation of the threshold slopes. Once a satisfactory approximation to the pair of threshold slopes of a lateral are computed based on Eqns. 6 and 7, the determination of the pressure head profile pattern (and possibly the locations of the pressure head extrema along the lateral) corresponding to any given lateral slope would then be reduced to a process of comparing the slope with the threshold slopes. In other words, no hydraulic simulation is needed for each new lateral slope. This is an advantage, because it will considerably simplify the process by which lateral pressure head profile patterns are determined as a function of lateral slopes. More significantly, however, the relationship between lateral threshold slopes and pressure head profile patterns can be used to develop simple and well-defined criteria for categorization of lateral pressure head profile patterns, as a function of slope, in a manner analogous to that presented in Table 1. This will enhance the practical utility of the results of the current study in such areas as verification of lateral hydraulic simulation models and design recommendations.

Evidently, the observations made here based on the results of the simulation study are essentially empirical and as such their application is limited to the data sets considered here. However, the fact that these data sets cover a wide range of lateral hydraulic, geometric, and slope characteristics (and hence a broad range of friction slopes and pressure slopes) strongly suggests that the inferences drawn here, with regard to the uniqueness of lateral threshold slopes and the relationship between lateral slope subintervals and pressure head profile patterns, may have a broader scope of application than just the data sets considered in the current study. Nonetheless, more comprehensive simulation studies are needed to conclusively establish this.

Irrigation laterals in modern farming systems are typically operated in a slope range that spans the upper end of the subinterval $\psi_l < \psi_i < \psi_u$ and the lower end of the subinterval $\psi_u \leq \psi_i$. Thus, in practice one may commonly encounter only a subset of the profile patterns described here. However, it is important to note that this has no bearing on the validity of the results presented here. These results cover a broader lateral slope range and hence represent a more comprehensive characterization of slope effects on lateral pressure head profile patterns.

Summary and Conclusions

Theoretical analysis of slope effects on the spatial patterns of lateral pressure head profiles is presented in the companion paper for a lateral with a spatially invariant parameter set. Results of the theoretical analysis are evaluated here based on hydraulic simulations. Accordingly, a simulation study was conducted based on three different data sets covering a wide range of lateral hydraulic and geometric characteristics. For each data set, multiple simulations were performed with a numerical hydralic model, by varying the lateral slope over a sufficiently wide interval such that the resultant pressure head profile patterns cover the full range of variation defined in the companion manuscript.

The simulation results show that the pressure head profile patterns of a lateral, and possibly the locations of the pressure head extrema along the lateral, can be determined based on a comparison of the negative of the lateral slope with the corresponding friction slopes at the inlet and/or distal ends of the lateral. Note that this result confirms an important inference of the theoretical analysis. The outcomes of the simulation study also show that the full range of variation of the pressure head profile patterns of a lateral can be differentiated into the three distinct categories defined in the companion paper based on theory.

Furthermore, additional insights, of some practical significance, into the relationships between lateral slopes and pressure head profile patterns stemming from the simulation study are summarized here. For each of the data set considered, the results reveal that there exists a unique pair of threshold slopes (referred here as the lower and upper lateral threshold slopes) that delimits the range of variation of the lateral slope into three subintervals, each with a specific pressure head profile pattern. The results also show that the spatial pattern of the simulated pressure head profiles, within each slope subinterval, corresponds to one of the three categories defined in the companion paper. Accordingly, category *I* pressure head profile pattern is observed for lateral slopes that are equal or less than the lower threshold slope. For slopes that vary between the lower and upper threshold slopes, the simulated pressure head profiles show category *II* pattern. For lateral slopes that exceed or equal the upper threshold slope, the corresponding pressure head profiles are of category *III* pattern.

The theoretical development presented in the companion paper is generally true. However, it produces only particular solutions that are specific to a lateral slope. By comparison, results of the simulation study suggest that the full range of variation of the pressure head profile patterns of a lateral can be completely characterized based on a pair of threshold slopes that are unique to a lateral. This will simplify the process by which lateral pressure head profile patterns are determined, as a function slope, and enhance the practical application of the outcomes of the theoretical analysis in such areas as verification of lateral hydraulic models and design recommendations. Evidently, the inferences deduced here based on the simulation study are empirical and hence in the strictest sense applicable only to the data sets considered in the current study. Thus, more comprehensive simulation studies might be needed in order to ascertain the broader practical significance of these results.

References

1. Warrick AW, Yitayew M (1988) Trickle Lateral Hydraulics. I: Analytical Solution. J Irrig Drain Eng 114: 281-288.
2. Wu PI (1992) Energy Gradient Line Approach for Direct Hydraulic Calculation in Drip Irrigation Design. Irrig Sci 13: 21-29.
3. Scaloppi EJ, Allen RG (1993) Hydraulics of Irrigation Laterals: Comparative Analysis. J Irrig Drain Eng ASCE 119: 91-115.
4. Vallesquino P, Luque-Escamilla PL (2002) Equivalent Friction Factor Method for Hydraulic Calculation in Irrigation Laterals. J Irrig Drain Eng 128: 278-286.
5. Tabuada MA (2014) Friction Head Loss in Center-Pivot Laterals with a Single Diameter and Multidiameter Lateral. J Irrig Drain Eng.
6. Zerihun D, Sanchez CA (2017) Irrigation Lateral Hydraulics with the Gradient Method. J Irrig. Drain Eng, ASCE.
7. Yitayew M, Warrick AW (1988) Trickle Lateral Hydraulics. II: Design and Examples. J Irrig Drain Eng 114: 289-300.
8. Keller J, Bliesner RD (1990) Sprinkle and Trickle Irrigation. Van Nostrand Reinhold, New York.
9. Anwar AA (1999) Adjusted Factor G_a for Pipelines with Multiple Outlets and Outflow. J Irrig Drain Eng ASCE 125: 355-359.
10. Valiantzas JD (2003) Explicit Hydraulic Design of Microirrigation Submain Units with Tapered Manifold and Lateral. J Irrig Drain Eng 129: 227.
11. Martin DL, Kincaid DC, Lyle WM (2007a) Chapter 16. Design and Operation of Sprinkler Systems. In: Design and Operation of Farm Irrigation Systems (2nd Ed) Hoffmann GJ, Evans RG, Jensen ME, Martin DL, Elliott RL (Eds.), ASABE, St. Joseph, MI, pp: 557-631.
12. Yildrim G (2015) Computer Based Analysis of Hydraulic Design Variables for Uniformly Sloping Microirrigation System Laterals. J Irrig Drain Eng.

13. Zerihun D, Sanchez CA, Baustista E (2018) Slope Effects on the Pressure Head Profile Patterns of Sprinkler Irrigation Laterals. II. Evaluation Based on Simulation. Submitted to Journal of Irrigation and Drainage Systems Engineering.

14. Wu IP, Saruwatari CA, Gitlin HM (1983) Design of Drip Irrigation Lateral Length on Uniform Slopes. Irrig Sci 4: 117-135.

15. Yildirim G (2007) Analytical Relationships for Designing Multiple Outlets Pipe Lines. J. Irrig. Drain. Eng 133: 140.

16. Martin DL, Heermann DF, Madison M (2007b) Chapter 15. Hydraulics of Sprinkler and Microirrigation Systems, In: Design and Operation of Farm Irrigation Systems, (2ndedn), Hoffmann GJ, Evans RG, Jensen ME, Martin DL, Elliott RL (Eds.), ASABE, St. Joseph, MI, pp: 532-555.